

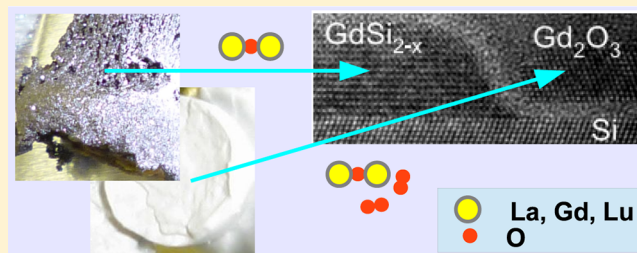
Oxygen-Deficient Oxide Growth by Subliming the Oxide Source Material: The Cause of Silicide Formation in Rare Earth Oxides on Silicon

Oliver Bierwagen,^{*,†} André Proessdorf,[†] Michael Niehle,[†] Frank Grosse,[†] Achim Trampert,[†] and Max Klingsporn[‡]

[†]Paul-Drude-Institut für Festkörperelektronik, Hausvogteiplatz 5-7, 10117 Berlin, Germany

[‡]IHP, Im Technologiepark 25, 15236 Frankfurt (Oder), Germany

ABSTRACT: The fundamental issue of oxygen stoichiometry in oxide thin film growth by subliming the source oxide is investigated by varying the additionally supplied oxygen during molecular beam epitaxy of RE_2O_3 ($\text{RE} = \text{Gd}, \text{La}, \text{Lu}$) thin films on Si(111). Supplying additional oxygen throughout the entire growth was found to prevent the formation of rare earth silicides observed in films grown without an oxygen source. Postgrowth vacuum annealing of oxygen stoichiometric films did not lead to silicide formation thereby confirming that the silicides do not form as a result of an interface instability at growth temperature in vacuum but rather due to an oxygen deficiency in the source vapor. The average oxygen deficiency of the rare-earth containing species in the source vapor was quantified by the ^{18}O tracer technique and correlated with that of the source material, which gradually decomposed during sublimation. Therefore, any oxide growth by sublimation of the oxide source material requires additional oxygen to realize oxygen stoichiometric films.



INTRODUCTION

Rare-earth oxides have a variety of physical properties that are important ingredients for application in future (opto)electronic devices on silicon substrates. Their chemical stability in contact with silicon enables suitable oxide buffer layers for integration of non-silicon-based semiconductors on silicon substrates.¹ Rare-earth (RE) oxides exhibit a high dielectric constant and a large band gap, which is the physical basis to be suitable as gate oxides in future CMOS devices.²

Most of these applications benefit from single crystalline oxide layers on silicon, for which molecular beam epitaxy (MBE) is a well suited deposition technique. In principle, two different growth schemes can be used for the oxide growth by MBE, or analogous deposition techniques. First is the thermal evaporation of the rare-earth metal with simultaneous addition of oxygen to form the oxide on the heated Si substrate,^{3–5} which allows a relatively low source temperature for the metal evaporation. This scheme bears the risk of detrimental effects of the free oxygen, such as formation of a parasitic SiO_2 interface layer, the degradation of hot filaments in the growth chamber, and the risk of silicide formation by reaction of the rare earth metal vapor with the heated silicon.⁶ The second is the thermal sublimation of the oxide itself with the source oxide vapor condensing on the heated Si substrate,^{1,7–11} which requires significantly higher temperatures than the evaporation of the rare-earth metal. This sublimation bears the promise to prevent silicide formation and to suffice without an additional oxygen

flux as depicted in Figure 1a with the source vapor consisting of stoichiometric RE_aO_b ($b/a = 3/2$) molecules.

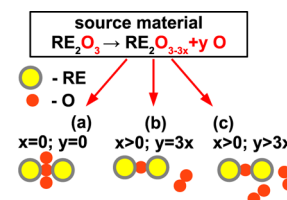


Figure 1. Schematic representation of sublimation modes of a rare-earth sesquioxide material RE_2O_3 : (a) Sublimation of stoichiometric molecules. (b) Stoichiometry-conserving sublimation of on-the-average O-deficient molecules (REO , RE) and associated free oxygen. (c) Nonstoichiometric sublimation (coincident with a decomposition) of O-deficient molecules (REO, RE) and more oxygen. This mode results in an effective oxygen depletion of the source material.

Experiments showed, however, that MBE growth without additional oxygen even from oxide sources of Nd_2O_3 ,⁷ Pr_2O_3 ,^{8,9} and Gd_2O_3 ^{10,12} can lead to the formation of interface silicide. This silicide formation has been attributed to its energetic preference over a stable Si-rare-earth-oxide interface at low oxygen chemical potential^{7–9} or to the interdiffusion of Gd and

Received: April 29, 2013

Revised: June 12, 2013

Published: July 10, 2013

Si at the interface of oxygen-deficient Gd_2O_3 layers and Si.¹⁰ In a review on rare earth oxides,¹³ their vaporization has been described to be stoichiometry-conserving as $\text{RE}_2\text{O}_3(\text{solid}) \rightarrow c\text{REO}(\text{gaseous}) + (2-c)\text{RE}(\text{gaseous}) + (3-c)\text{O}(\text{gaseous})$ [0 < $c < 2.0$], schematically shown in Figure 1b. The presence of a rare-earth metal vapor in this case might already explain the observed silicide formation. The nonstoichiometric vaporization with oxygen loss, schematically shown in Figure 1c, has been recently described in ref 12. During (electron-beam) sublimation of fresh Gd_2O_3 source material, silicide-free Gd_2O_3 layers were grown on Si(001) even without additional oxygen. However, additional oxygen to prevent silicide formation was required during subsequent growth runs, which was attributed to a significant oxygen loss of the source material during sublimation (which likely served as source of oxygen in the first sample(s)).

In this paper, we find silicide formation during growth on silicon due to a lack of oxygen in the oxide source vapor in the case of La_2O_3 , Gd_2O_3 , and Lu_2O_3 . With the example of Gd_2O_3 , we also show that the $\text{Gd}_2\text{O}_3/\text{Si}(111)$ interface is stable under vacuum at growth temperature and that an additional oxygen supply is required to prevent silicide formation not only during interface formation but also during the growth of the entire layer. The average oxygen deficiency of the rare-earth containing species in the oxide vapor was further investigated by an oxygen isotope tracer technique. All results indicate a sublimation of the source oxide according to the schematics of Figure 1c, that is, with suboxide molecules RE_aO_b ($b/a < 3/2$) in the vapor and coincident oxygen depletion (by decomposition) of the source material. These results show the fundamental necessity of providing additional oxygen to realize oxygen stoichiometric oxide films when sublimating oxide source materials.

EXPERIMENTAL SECTION

All samples used in this study were grown by molecular beam epitaxy (MBE) on the (7 × 7)-reconstructed Si(111) surface at a substrate temperature of 700 °C (measured by a thermocouple between substrate and substrate heater). The La_2O_3 , Gd_2O_3 , and Lu_2O_3 source materials were sublimated by special high-temperature effusion cells (TUBO) at cell temperatures of around 1600, 1700, and 1800 °C, respectively. These temperatures were measured by thermocouples not in contact with the tantalum crucibles. Therefore, the actual crucible temperature could be somewhat higher. The resulting growth rate was on the order of 0.1 ML/min (1 ML = 3.1 Å = 1 monolayer). To investigate the role of oxygen, the injection of molecular oxygen during growth was chosen to be $(1-2) \times 10^{-7}$ mbar ("with O_2 ") or $< 10^{-11}$ mbar ("no O_2 "). Oxygen injection was started at growth temperature and 30 s prior to oxide growth. Further experimental details are given in ref 14.

In situ reflection high-energy electron diffraction (RHEED) measurements were used to determine surface morphology during growth. A streaky RHEED pattern is indicative of a smooth surface, whereas a spotty RHEED pattern, which arises from the transmission diffraction of the electron beam through three-dimensional surface structures, would indicate a rough surface. After growth, the surface morphology was investigated by atomic force microscopy (AFM), and the crystal phases present in the samples were identified by X-ray diffraction (XRD) with an open detector using Cu K α radiation and in selected samples by cross-sectional transmission electron microscopy (TEM).

RESULTS AND DISCUSSION

Silicide Formation without Additional Oxygen Supply. The first set of experiments was conducted in the absence

of additional oxygen. Oxide films grown under these conditions were found to contain silicides. By contrast, in the presence of additional oxygen, smooth, silicide-free rare-earth oxide films were grown for La_2O_3 , Lu_2O_3 , and (as already demonstrated in refs 10 and 12) Gd_2O_3 . Figure 2 summarizes our experimental results. Figure 2 (top) shows the symmetric $2\Theta-\omega$ XRD scans with the major peaks labeled with the corresponding crystal and orientation. Below the XRD spectra in Figure 2, the associated film morphologies are shown by AFM images for Gd_2O_3 and

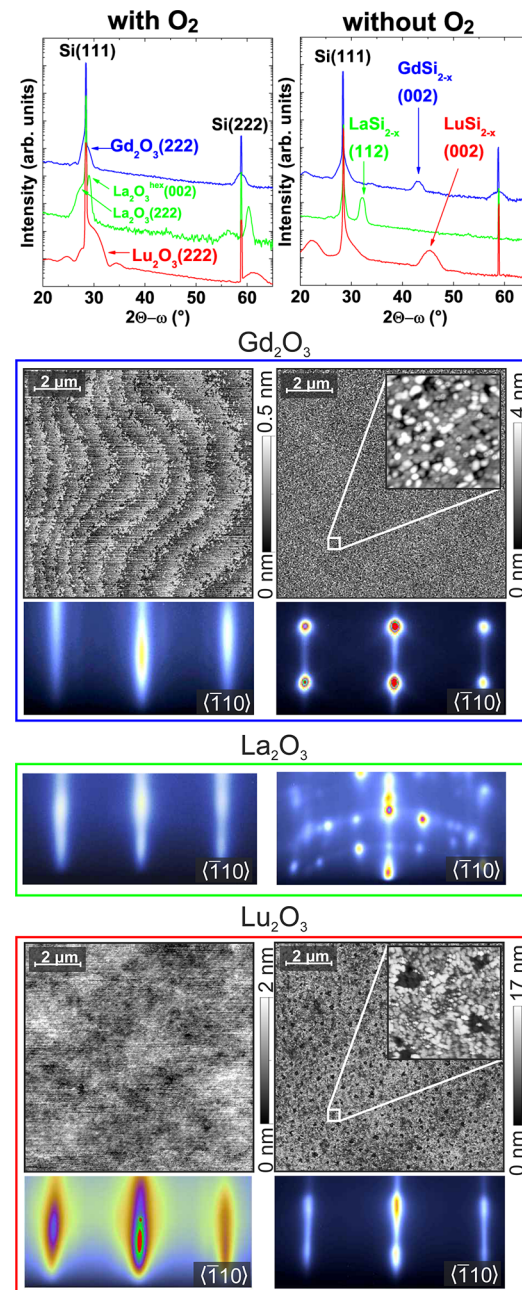


Figure 2. Comparison of crystal phases and surface morphology of Gd_2O_3 , La_2O_3 , and Lu_2O_3 films on Si(111) grown with O_2 (left) and without O_2 (right). (Top) XRD $2\Theta-\omega$ scans to identify crystal phases (labeled) present in the film. For the La_2O_3 grown with O_2 , a cubic and a hexagonal phase are present. (Bottom) RHEED and AFM images indicating the surface morphology. AFM was not measured for the La_2O_3 film, which is unstable in air and had to be protected by an amorphous Si cap layer.

Lu_2O_3 and by RHEED patterns collected after film growth for all three oxides.

The XRD scans of the films grown with additional oxygen clearly show peaks of (111) oriented rare-earth oxides. The rare-earth oxides La_2O_3 ($a = 1.14 \text{ nm}$),¹⁵ Gd_2O_3 ($a = 1.082 \text{ nm}$),¹⁶ and Lu_2O_3 ($a = 1.04 \text{ nm}$)¹⁷ assume a bixbyite (cubic) crystal structure (space group 206, $I\bar{a}3$) during deposition on Si(111).^{11,18} In the case of La_2O_3 only, an additional hexagonal structure (space group 164, $P\bar{3}m1$, $a = 0.39 \text{ nm}$, $c = 0.61 \text{ nm}$)¹⁹ is observed. Due to the close lattice match to the substrate, the Gd_2O_3 film is visible as a broad peak with thickness fringes underneath the sharp Si substrate peaks. For La_2O_3 and Lu_2O_3 , the oxide film peaks are slightly offset from the substrate peak. The nominally 3 nm-thick Gd_2O_3 and Lu_2O_3 films grown with oxygen show a smooth surface. This is demonstrated in the AFM images and by the streaky RHEED patterns. A streaky RHEED pattern also confirms the smoothness of the nominally 20 nm-thick La_2O_3 film.

In contrast, the corresponding films grown without oxygen ("no O_2 ") show additional XRD peaks and a rough morphology (see magnified AFM and spotty RHEED patterns). Both these results suggest a formation of another crystalline phase, which could be a silicide or a silicate. Various crystal structures for rare-earth silicides are reported in the literature. For the Gd_2O_3 film grown without oxygen, the high-resolution cross-sectional transmission electron microscopy (HRTEM) images (Figure 3b) and XRD measurements (further lattice planes not shown) are consistent with the reported data for the silicide GdSi_{2-x} with space group 191 ($P\bar{6}/mmm$) and lattice parameters $a =$

0.387 nm and $c = 0.418 \text{ nm}$.²⁰ This assignment was further corroborated in a sample with Gd (metal) deposited on Si(111) at the same substrate temperature of 700°C where identical XRD peaks appeared. LuSi_{2-x} with the same crystal structure (space group 191 ($P\bar{6}/mmm$), lattice parameters $a = 0.375 \text{ nm}$, $c = 0.405 \text{ nm}$)²¹ and orientation as the GdSi_{2-x} was formed in the Lu_2O_3 film grown without oxygen as evidenced by the almost identical XRD peaks and transmission diffraction spots in the RHEED pattern. For the nominally 20 nm-thick La_2O_3 film, the spotty RHEED pattern and the XRD peaks differ from those of the Gd_2O_3 and Lu_2O_3 films, which indicates a different silicide crystal structure or orientation. In fact, the crystal structure of LaSi_{2-x} deviates from the other two. The closest match is found for the reported crystal structure having space group 141 ($I4_1/and O2$) and lattice parameters are $a = 0.43 \text{ nm}$ and $c = 1.38 \text{ nm}$.²²

Our results, together with published results on other rare-earth oxides, confirm the general trend of silicidation during MBE growth of rare-earth oxides on silicon from the oxide source without an additional supply of oxygen.

Interface Stability with Respect to Silicidation: The Example of Gd_2O_3 . To determine whether the presence of the silicide is solely related to the interface formation, a cross-sectional TEM study and further growth experiments were performed with Gd_2O_3 . In Figure 3a, TEM images of Gd_2O_3 grown with additional oxygen shows a sharp and planar interface between the Si and the Gd_2O_3 film. The growth without additional oxygen, in contrast, results in GdSi_{2-x} inclusions in the oxide film and in the substrate as shown in Figure 3b. All of the results so far suggest the presence of silicides to be related to the interface formation in the absence of oxygen as described in ref 7.

In an additional growth experiment, a nominally 6 nm-thick Gd_2O_3 layer deposited with oxygen was capped by another 6 nm-thick Gd_2O_3 layer grown without oxygen. With this growth scheme, oxygen is supplied to prevent silicidation during the interface growth, which was confirmed by a streaky RHEED pattern. Unexpectedly, in Figure 4, the resulting XRD scan again indicates GdSi_{2-x} formation, and the AFM image shows a smooth film with a pore-like roughness on the micrometer-scale. In this sample, though, the GdSi_{2-x} must have formed during the deposition of the top "6 nm without oxygen". Cross-sectional TEM images of the film in Figure 3c show a continuous oxide film with "pores" that likely consist of the silicide. This silicide formation could be explained either by oxygen loss and following interfacial reaction of the bottom 6 nm film with the substrate or by the reaction of the incoming " Gd_2O_3 "-vapor with the substrate through the bottom film.

A reference sample consisting of a nominally 6 nm thick film grown with oxygen directly followed by a vacuum anneal at growth temperature ("6 nm with $\text{O}_2 + \text{vacuum anneal}$ ") for the same time as the growth of the top layer in the previous sample showed a smooth morphology and the absence of a GdSi_{2-x} peak in XRD as shown in Figure 4. This result demonstrates that the $\text{Gd}_2\text{O}_3/\text{Si}(111)$ interface itself is stable against silicidation under vacuum at growth temperature. Therefore, in the previous sample, the incoming " Gd_2O_3 "-flux formed the silicide with Si atoms from the substrate by diffusion of Gd metal from the source vapor and Si from the substrate (which both form the silicide) through the bottom 6 nm Gd_2O_3 layer in the location of the pores. We speculate that the location of the pores coincides with defective regions of the 6 nm Gd_2O_3 bottom layer that form easy vertical diffusion channels. In this

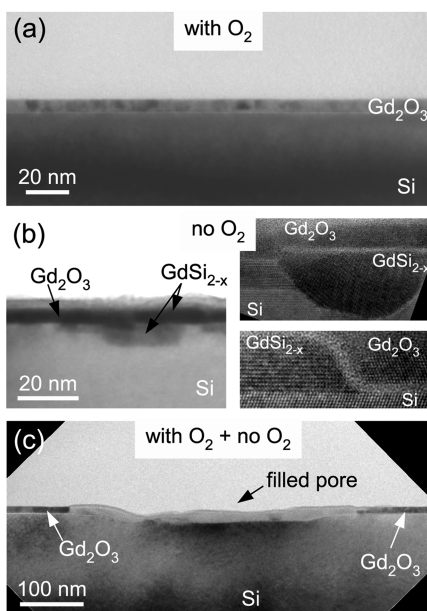


Figure 3. TEM bright field images of Gd_2O_3 grown under different oxygen flux (a) with O_2 , reflecting a smooth layer without an interface roughening due to chemical reactions (contrast fluctuations in the thin film point to heterogeneity in the crystallinity); (b) without O_2 , reflecting a rough interface region with in-diffusion in Si substrate and different phases in layer; HRTEM insets illustrate in-diffused part, partly overgrown by Gd_2O_3 phase (upper image) and coexistence of GdSi_{2-x} and Gd_2O_3 phase in thin film (lower one), horizontal lattice fringes in the substrate correspond to Si(111) planes (0.31 nm); (c) with $\text{O}_2 + \text{no O}_2$, two beam case with $g = (111)_\text{Si}$, reflecting a smooth Gd_2O_3 layer interrupted by pores; pore filling is crystalline (not shown here).

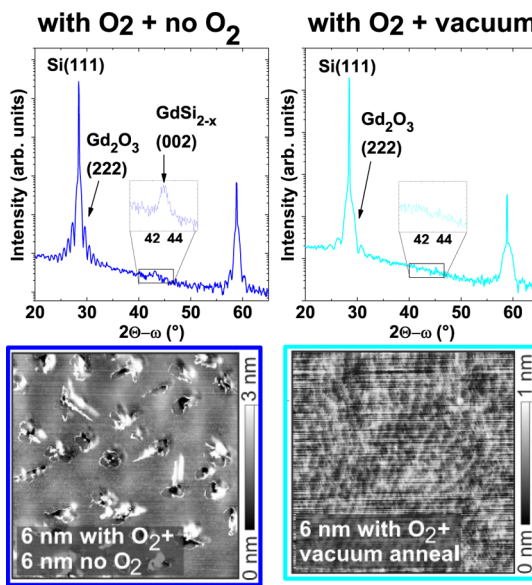


Figure 4. XRD 2θ- ω scans (top) of a Gd₂O₃ films after annealing in (left, dark blue) “Gd₂O₃-vapor” and (right, light blue) vacuum, no flux. The inset shows the magnified silicide peak. Below the corresponding AFM images are shown.

case, the areal density of the pores could be a quantitative measure for this defect density.

A more important corollary of the above results, however, is that the “Gd₂O₃” vapor contains Gd metal (without bonded oxygen) that forms the silicide with silicon from the substrate.

Oxygen Tracer Technique To Confirm and Quantify Source Vapor Oxygen Deficiency. As a more direct way to determine the amount of oxygen deficiency in the source oxide vapor, we used the isotope tracer technique, a technique that has already been demonstrated for the study of the SnO₂ growth kinetics.²³ The concept of this technique is schematically shown in Figure 5: Isotope pure oxygen ¹⁸O₂ with a

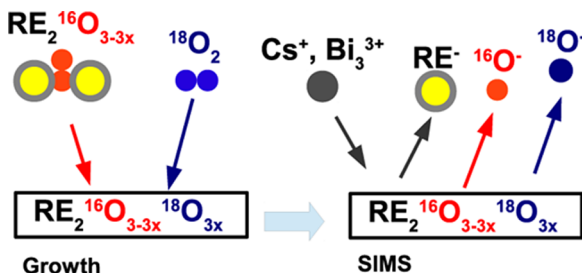


Figure 5. Schematics of the oxygen tracer technique used to determine the oxide vapor oxygen deficiency. (left) Missing ¹⁶O from the source vapor is replaced by the supplied, isotope pure ¹⁸O during the formation of the (approximately) oxygen stoichiometric rare-earth oxide film. (right) The amount of ¹⁸O relative to ¹⁶O in the grown film is measured by secondary ion mass spectroscopy, allowing further inference on the O-deficiency of the source vapor.

natural abundance of ~0.2% was used as the additional oxygen source during the oxide film growth. This isotope pure oxygen incorporated into the film for the missing ¹⁶O (natural abundance ~99.8%) in the source oxide vapor. More specifically, this ¹⁸O incorporated for the missing oxygen in the rare-earth containing species of the source vapor as evidenced by mass spectra of the gases in the growth chamber

during the isotope tracer experiments, which showed that the amount of free natural oxygen (¹⁶O₂), for example, from the source vapor, is negligible in comparison to the additionally supplied ¹⁸O₂. After growth, time-of-flight secondary ion mass spectroscopy (ToF-SIMS) measured the ¹⁸O proportion of the entire O-content of the films, which is an estimate of the oxygen in the grown film not originating from the oxide source. In order to determine the vapor oxygen stoichiometry, the results had to be corrected for ¹⁸O proportions in the film that arose from the oxygen exchange process (¹⁶O \leftrightarrow ¹⁸O) of the oxide film with the surrounding ¹⁸O atmosphere.

Dedicated ~6 nm-thick Gd₂O₃, La₂O₃, and Lu₂O₃ films were grown in ~10⁻⁷ mbar ¹⁸O₂ at a reduced substrate temperature of 350 °C to minimize the impact of oxygen exchange between film and gas. To estimate the contribution of oxygen exchange for each of these oxides, a reference film was grown under the same conditions but with ~10⁻⁷ mbar ¹⁶O₂ and was subsequently annealed at growth temperature in ~10⁻⁷ mbar ¹⁸O₂ for the same time as the layer growth. As an example, Figure 6 shows the SIMS profiles of the oxygen isotopes and Si

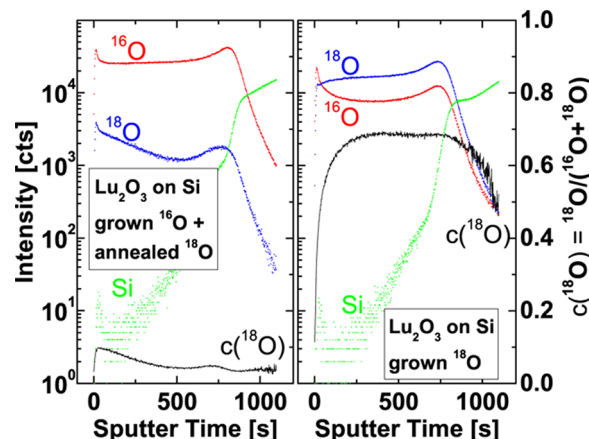


Figure 6. ToF-SIMS profiles of ¹⁸O (blue, left scale), ¹⁶O (red, left scale), and ²⁸Si (green, left scale) in a Lu₂O₃ film grown with ¹⁸O (right). The contribution of oxygen exchange was estimated with a reference film (left). The ¹⁸O proportion, *c*(¹⁸O), of the total oxygen amount is shown with the profiles (black line, right scale).

in the Lu₂O₃ film and the associated reference film. The profile depth is proportional to the sputter time: 0 s corresponds to the surface, and the peaking O-intensity along with the plateauing Si-intensity at ~750–800 s indicate the oxide–Si interface. For the quantitative analysis, the surface and interface regions (0–50 s and last 50 s before O-peak, corresponding to slabs of ~1.5 ML) are excluded to prevent the influence of surface and interface impurities. The ¹⁸O proportion of the total oxygen content “*c*(¹⁸O)” is calculated as *c*(¹⁸O) = *I*(¹⁸O)/[*I*(¹⁶O) + *I*(¹⁸O)] with measured intensities *I*(¹⁶O) and *I*(¹⁸O) for the respective oxygen isotopes and is shown in Figure 6.

The average *c*(¹⁸O) from the remaining (inner) part of the films is *c*_{film}(¹⁸O) = 0.666 and *c*_{ref}(¹⁸O) = 0.065 for the Lu₂O₃ film and reference, respectively. The proportion of ¹⁸O due to the vapor oxygen deficiency (cf. Figure 5) is calculated as *x* = *c*_{film}(¹⁸O) – *c*_{ref}(¹⁸O). For the Lu₂O_{3-3x} we find *x* = 0.6, which means that more than half the oxygen is missing. The same analysis yields *c*_{film}(¹⁸O) = 0.231 and 0.213, *c*_{ref}(¹⁸O) = 0.039 and 0.065, and *x* = 0.19 and 0.15 for Gd₂O₃ and La₂O₃, respectively.

Therefore, the oxygen isotope tracer technique confirmed that under the chosen experimental conditions an oxygen-deficient incorporation from the source oxide vapors with an average stoichiometry of $\text{Gd}_2\text{O}_{2.43}$, $\text{La}_2\text{O}_{2.55}$, and $\text{Lu}_2\text{O}_{1.2}$ occurs.

Sublimation and Decomposition of the Rare-Earth Oxides. The scenarios of rare-earth oxide sublimation shown in Figure 1 will be discussed based on the above quantitative results and the following assumptions: First, molecules that consist of RE and O atoms (RE_aO_b) will condense on the substrate (have a sticking coefficient of unity) and incorporate into the film without splitting off any O. (The O would have split off at the source rather than at the substrate because the source temperature is much higher than that of the substrate.) Second, we assume O_2 molecules (additionally supplied or from the source vapor) to have a sticking coefficient of less than unity.

Under these assumptions, sublimation of only stoichiometric ($b/a = 3/2$) rare-earth oxide molecules (of Figure 1a) can be ruled out because it would not lead to silicide formation in the absence of oxygen.

The stoichiometry-conserving sublimation with on-the-average oxygen-deficient rare-earth oxide molecules with ($b/a < 1$) shown in Figure 1b), in contrast, would in fact lead to silicide formation under the absence of oxygen because not all free oxygen from the source vapor would incorporate into the film. This scenario can, however, be ruled out because ref 12 and our observations show an increasing oxygen deficiency of the source material after successive growth runs. Figure 7 shows photographs of the source material after a different number of growth runs. The stoichiometric source material is white and turned gray and black and finally shows macroscopic metallic

particles, which is a clear indication of successive oxygen depletion.

Hence, sublimation of on-the-average oxygen-deficient rare-earth oxide molecules with simultaneous decomposition of the source material (Figure 1c), adding free oxygen to the source vapor, explains all our results. A sufficiently high amount of this free oxygen in the source vapor could explain the absence of silicide formation during the growth of Gd_2O_3 on Si by electron-beam sublimation of the fresh source material mentioned in ref 12. In addition, a rapid decrease of the free oxygen content in the source vapor due to the oxygen depletion of source materials explains the necessity of additional oxygen during subsequent growth to prevent silicide formation as found in ref 12.

Based on the average stoichiometry (b/a) determined by the oxygen tracer technique, we can give estimates for the stoichiometry of the rare-earth containing species in the oxide vapor: The stoichiometry of $\text{Gd}_2\text{O}_{2.43}$ and $\text{La}_2\text{O}_{2.55}$ corresponds to $b/a \approx 1.25$. This value is larger than the range $0 < b/a < 1$ given in ref 13 (mixture of REO and RE) and can only be explained by a significant fraction of rare-earth oxide molecules with $b/a > 1.25$, for example, RE_2O_3 or REO_2 , in the source vapor. In contrast, the average stoichiometry of $\text{Lu}_2\text{O}_{1.2}$ with $b/a = 0.6$ suggests large amounts of metallic Lu in the vapor, which is consistent with the metallic fraction visible in the photograph of the used source material (Figure 7, bottom left).

SUMMARY AND CONCLUSION

In summary, we have shown in the cases of La_2O_3 , Gd_2O_3 , and Lu_2O_3 , that an oxygen-deficient growth mechanism and not an interface instability causes rare earth silicide formation during sublimation of rare earth oxides on silicon. Interfacial silicides are formed when rare earth oxides are sublimated onto heated silicon in vacuum at the chosen substrate temperature. To prevent the formation of the silicide, additional oxygen has to be supplied to compensate for the vapor oxygen deficiency. We demonstrated through the example of Gd_2O_3 that this oxygen supply is necessary not only during interface formation but also during the layer growth since rare earth metal from the source vapor or silicon from the substrate was found to diffuse through an existing rare earth oxide layer, likely in defective regions, and form a silicide.

The rare-earth oxides were found to sublime by emitting on-the-average oxygen-deficient rare-earth containing species RE_aO_b ($b/a < 3/2$) and by coincident decomposition with the emission of free oxygen. The average oxygen deficiency of the rare-earth containing species in the source vapor was quantified by the isotope tracer technique. Based on the quantitative results, a large proportion of rare-earth metal existed in the vapor of the strongly oxygen depleted source material Lu_2O_3 , which had a visible metallic fraction. The less oxygen depleted La_2O_3 and Gd_2O_3 sources, in contrast, must have emitted a significant fraction of species with ($b/a > 1$), possibly stoichiometric RE_2O_3 .

Our qualitative results likely apply to all physical vapor deposition techniques that are based on the sublimation of any oxide source material. The supply of additional oxygen during growth is necessary to obtain a stoichiometric oxide film.

AUTHOR INFORMATION

Corresponding Author

*E-mail: bierwagen@pdi-berlin.de.

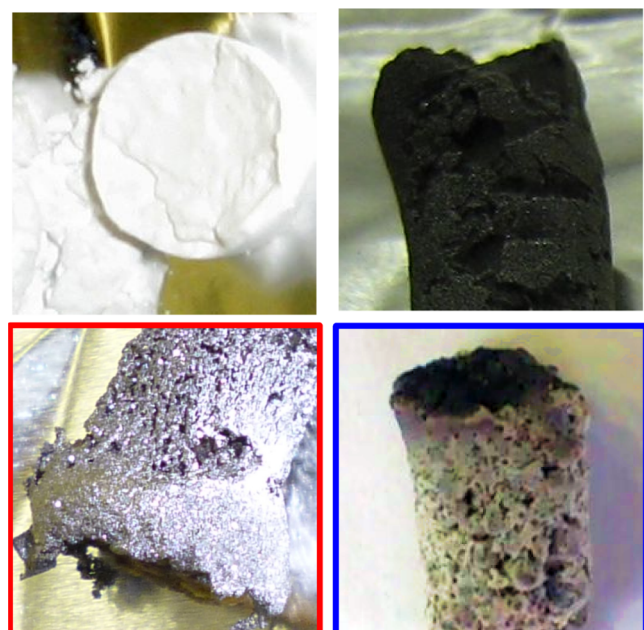


Figure 7. Photographs of the source materials. (top left) fresh, white Lu_2O_3 powder. (top right) the same Lu_2O_3 powder after a number of growth runs turned black. (bottom left) The same Lu_2O_3 powder after significantly more growth runs shows a metallic surface. This source material was used for the present study. (bottom right) The Gd_2O_3 source material, gray after a number of growth runs, used for this study.

Notes

The authors declare no competing financial interest.

ACKNOWLEDGMENTS

We would like to thank T. Schröder for valuable discussion, M. Lopes for critically reading the manuscript, S. Behnke and C. Stemmler for technical support, and J. Dinner for proofreading. This work was supported by the Leibniz-Gemeinschaft under the Project No. SAW-2011-PDI-230.

REFERENCES

- (1) Giussani, A.; Zaumseil, P.; Seifarth, O.; Storck, P.; Schroeder, T. *New J. Phys.* **2010**, *12*, No. 093005.
- (2) Schlom, D. G.; Guha, S.; Datta, S. *MRS Bull.* **2008**, *33*, 1017–1025.
- (3) Guha, S.; Cartier, E.; Gribelyuk, M. A.; Bojarczuk, N. A.; Copel, M. C. *Appl. Phys. Lett.* **2000**, *77*, 2710–2712.
- (4) Dargis, R.; Arkun, E.; Clark, A.; Roucka, R.; Smith, R.; Williams, D.; Lebby, M.; Demkov, A. A. *J. Vac. Sci. Technol., B: Microelectron. Nanometer Struct.-Process., Meas., Phenom.* **2012**, *30*, No. 02B110.
- (5) Grave, D. A.; Hughes, Z. R.; Robinson, J. A.; Medill, T. P.; Hollander, M. J.; Stump, A. L.; Labella, M.; Weng, X.; Wolfe, D. E. *Surf. Coat. Technol.* **2012**, *206*, 3094–3103.
- (6) Zhu, Y.; Xu, R.; Chen, S.; Fang, Z.; Xue, F.; Fan, Y.; Yang, X.; Jiang, Z. *Thin Solid Films* **2006**, *508*, 86–89.
- (7) Fissel, A.; Ellassar, Z.; Kirfel, O.; Bugiel, E.; Czernohorsky, M.; Osten, H. *J. Appl. Phys.* **2006**, *99*, 074105.
- (8) Watahiki, T.; Tinkham, B. P.; Jenichen, B.; Shayduk, R.; Braun, W.; Ploog, K. H. *Appl. Surf. Sci.* **2008**, *255*, 758.
- (9) Schaefer, A.; Zielasek, V.; Schmidt, T.; Sandell, A.; Schowalter, M.; Seifarth, O.; Walle, L. E.; Schulz, C.; Wollschlaeger, J.; Schroeder, T.; Rosenauer, A.; Falta, J.; Baumer, M. *Phys. Rev. B: Condens. Matter Mater. Phys.* **2009**, *80*, No. 045414.
- (10) Watahiki, T.; Jenichen, B.; Shayduk, R.; Tinkham, B. P.; Braun, W.; Riechert, H. *J. Cryst. Growth* **2009**, *311*, 2179.
- (11) Grosse, F.; Bokoch, S.; Behnke, S.; Proessdorf, A.; Niehle, M.; Trampert, A.; Braun, W.; Riechert, H. *J. Cryst. Growth* **2011**, *323*, 95–98.
- (12) Sitaputra, W.; Tsu, R. *Appl. Phys. Lett.* **2012**, *101*, No. 222903.
- (13) Adachi, G.-y.; Imanaka, N. *Chem. Rev.* **1998**, *98*, 1479–1514.
- (14) Hanke, M.; Kaganer, V.; Bierwagen, O.; Niehle, M.; Trampert, A. *Nanoscale Res. Lett.* **2012**, *7*, 203.
- (15) Gobichon, A.-e.; Auffrédic, J.-P.; Louér, D. *J. Solid State Chem.* **1999**, *144*, 68–80.
- (16) Heiba, Z.; Okuyucu, H.; Hascicek, Y. S. *J. Appl. Crystallogr.* **2002**, *35*, 577–580.
- (17) Samoylenko, S.; Gorbenko, O.; Kaul, A.; Rebane, Y.; Svetchnikov, V.; Zandbergen, H. *J. Alloys Compd.* **1997**, *251*, 342–346.
- (18) Watahiki, T.; Grosse, F.; Braun, W.; Kaganer, V. M.; Proessdorf, A.; Trampert, A.; Riechert, H. *Appl. Phys. Lett.* **2010**, *97*, No. 031911.
- (19) Gouteron, J.; Michel, D.; Lejus, A.; Zarembowitch, J. *J. Solid State Chem.* **1981**, *38*, 288–296.
- (20) Huang, M.; Schlagel, D. L.; Schmidt, F. a.; Lograsso, T. a. *J. Alloys Compd.* **2007**, *441*, 94–100.
- (21) Koleshko, V.; Belitsky, V.; Khodin, A. *Thin Solid Films* **1986**, *141*, 277–285.
- (22) Nakano, H.; Yamanaka, S. *J. Solid State Chem.* **1994**, *108*, 260–266.
- (23) Zhen, Y.; Ohsawa, T.; Adachi, Y.; Sakaguchi, I.; Li, B.; Li, J.; Matsuoka, R.; Nishimura, T.; Matsumoto, K.; Haneda, H.; Ohashi, N. *J. Appl. Phys.* **2010**, *108*, No. 104901.